Journal of Materials Chemistry A

ROYAL SOCIETY OF CHEMISTRY

PAPER

View Article Online
View Journal | View Issue

Cite this: J. Mater. Chem. A, 2024, 12, 9102

High-throughput screening and characterization of novel zeolitic imidazolate framework gels†

Izuru Miyazaki, Yumi Masuoka, Keiichiro Oh-Ishi, Norihiko Setoyama and Mitsutaro Umehara*

Metal–organic frameworks (MOFs) are promising electrochemical energy storage materials for batteries and supercapacitors, gas storage materials, and adsorption materials for adsorption heat pumps. An obstacle to their practical application is the conversion of powdered MOFs into bulk bodies. Using MOF gels is a promising method; however, to date, only a few MOF gels have been identified for synthesis, and a unified strategy for synthesizing the desired MOF gels is unclear. This study explored the gelation conditions for zeolitic imidazolate framework (ZIF) gel synthesis using acetate by efficiently targeting multiple ZIFs *via* high-throughput screening and subsequent batch synthesis. Here, novel ZIF-zni and ZIF-61 gels were synthesized and characterized. These gels formed dense and mechanically rigid films on multiple substrates *via* simple coating and drying processes. This process has excellent industrial feasibility; therefore, the results are critical for the practical application of ZIF-zni and ZIF-61 films on desired substrates. Moreover, the unique application of the potential of the obtained ZIF-zni and ZIF-61 gels as structural adhesives for metals was investigated. The shear strength of the adhesive exceeded 30 MPa. This value exceeds those of previously reported MOF adhesives. Furthermore, using data obtained from high-throughput screening experiments, the influence of the synthesis conditions on wet gel formation, which is crucial for the realization of gel-derived films and adhesives, was evaluated through statistical modeling. Several factors like reactant concentration were estimated to have statistically significant effects on gelation, which is critical in determining the widely applicable conditions for gelation.

Received 3rd November 2023
Accepted 4th March 2024

DOI: 10.1039/d3ta06719j

rsc.li/materials-a

1 Introduction

Advancing energy materials is an immediate need to overcome the energy crisis caused by a rapidly growing population and dependence on fossil fuels.[1,2] MOFs are porous crystalline materials composed of metal ions and organic ligands. Because of their controllable morphology, high specific surface area, and multifunctionality, they are expected to be electrochemical energy storage materials, for example, in batteries and supercapacitors, gas storage materials, and adsorption materials for adsorption heat pumps.[3–12]

Synthesized MOFs are often obtained as fine particles.[13] However, handling the powder form in industrial environments, such as pressure, temperature, and vacuum swing adsorption systems, is challenging. Hence, it is crucial to keep MOFs in a rigid bulk form to maintain reliable performance.[14–16]

The widely investigated method of bulking is the formation of films with suitable substrates as in the layer-by-layer method,[17–20] *in situ* synthesis,[21–23] sputter/atomic layer deposition,[24] chemical solution deposition,[25,26] chemical vapor deposition,[27] *etc.* Refer to papers[28–31] for a survey of these studies. Monolithic composites are also effective with silicone,[13] polymers of intrinsic microporosity (PIM),[32,33] polyvinylpyrrolidone (PVP),[34] polydimethylsiloxane (PDMS),[35] and poly(1,4-phenylene ether–ether–sulfone) (PPEES)[36] as binders. Rigid MOF composites with desired shapes can be obtained using binders with excellent plasticity and mechanical strength. More prior studies are detailed in ref. 14 and 37–39.

Pure MOF-only bulk bodies without binders have been actively studied owing to their superior volumetric performances. This includes monolithization by simple powder compaction[40] and MOF powder sintering by mild drying.[41,42] However, these methods have poor mechanical strength and industrial feasibility, respectively. Methods for forming films and monoliths using MOFs in the gel state or metal–organic gels (MOGs) have recently been proposed and are actively studied.[26,43–56] This method has attracted considerable attention owing to its potential to create bulk bodies with excellent mechanical strength using a variety of industrially feasible coating methods.[57,58]

Toyota Central R&D Labs., Inc., Nagakute, Aichi, Japan. E-mail: umehara@mosk.tytlabs.co.jp

† Electronic supplementary information (ESI) available. See DOI: https://doi.org/10.1039/d3ta06719j

However, the conditions required for forming MOF gels are not well understood. MOF gels consist of discrete crystalline nanoparticles forming a colloidal network through weak non-covalent interactions in the liquid phase. It is believed that smaller particle size is more favorable for gel formation. Therefore, the ease of gel formation in various MOFs is considered to be related to their crystallization behavior.[57] Nonetheless, the crystallization mechanism of MOFs has not been fully clarified because phenomena that cannot be explained by classical nucleation theory, such as a decrease in the crystallization rate of MOFs with increasing reactant concentration, have been reported.[59] In addition, experimental studies on the formation of MOF gels have shown that the formation of MOF gels is affected by the choice of metal source, presence of water, reactant concentration,[48] temperature,[54] presence of a base,[51] solvent,[60] *etc.*, and a unified strategy to determine the conditions for synthesizing the targeted MOF gels is not clear. Therefore, there are a limited number of MOFs for which gel synthesis methods are already known, as mentioned above. Recently, a sol–gel-derived film preparation method for the zeolitic imidazolate framework (ZIF), one of the most representative MOF classes and promising gas adsorbents, has been proposed.[26] Combining this method with the optimized temperature and pressure during the film preparation can lead to the formation of a structure with excellent mechanical strength.[61] These simple methods use acetate as the metal source for the capping effect of acetate ions and may apply to a wide range of ZIFs other than ZIF-67 and ZIF-8, as demonstrated in that study. However, as mentioned earlier, several factors are involved in the formation of MOF gels; hence, determining the conditions for the synthesis of a targeted MOF gel and forming its derived bulk body among the vast number of possible conditions is challenging.

High-throughput experiments (HTEs) and screening are powerful methods for this situation, allowing efficient validation of a significant number of experimental conditions.[62–64] So far, the usefulness of HTEs for MOFs has also been reported, although not in large numbers.[65–67]

Therefore, this study investigates the gelation conditions for ZIF gel synthesis using acetate by efficiently targeting multiple ZIFs *via* high-throughput screening and subsequent batch synthesis. We also clarify the properties of the obtained ZIF gels and gel-derived films and an evaluation of their mechanical properties. Furthermore, we report a unique application of this MOF gel: the strong adhesion of metals. This is related to the adhesion strength of the gel-derived film to the substrate, which is an essential mechanical property for mounting MOF devices. The influence of factors, such as reactant concentration and solvent, on gelation is clarified by statistical modeling, and a unified strategy for MOF gel fabrication is discussed.

2 Experimental

2.1 Materials

The target MOFs were a class of ZIFs including ZIF-2, ZIF-4, ZIF-zni, ZIF-10, ZIF-11, ZIF-12, ZIF-20, ZIF-21, ZIF-60, ZIF-61, ZIF-62, ZIF-64, ZIF-71, ZIF-72, ZIF-73, ZIF-74, ZIF-75. Zn^{2+} and Co^{2+}, which are typical metal ions in ZIFs, were used as the metal sources in the form of zinc acetate dihydrate (99.9%, Fujifilm Wako Pure Chemicals, ZnAc) and cobalt acetate tetrahydrate (99.0%, Fujifilm Wako Pure Chemicals, CoAc). Imidazole (98%, Fujifilm Wako Pure Chemicals, im), benzimidazole (98%, Fujifilm Wako Pure Chemicals, bim), 2-nitroimidazole (98%, Tokyo Chemical Industry, nim), 5,6-dimethylbenzoimidazole (99%, Tokyo Chemical Industry, dmim), 2-methylimidazole (98%, Fujifilm Wako Pure Chemicals, mim), 4,5-dichloroimidazole (97%, Tokyo Chemical Industry, dcim), and purine (95%, Fluorochem, pr) were used as the organic ligands. Sodium hydroxide (97%, Fujifilm Wako Pure Chemicals) and potassium hydroxide (85%, Fujifilm Wako Pure Chemicals) were used as the bases. Ethanol (99.5%, Fujifilm Wako Pure Chemicals), *N*,*N*-dimethylformamide (DMF, 99.5%, Fujifilm Wako Pure Chemicals), and deionized water were used as solvents. All reagents were used as received.

2.2 High-throughput screening for ZIF gels

The following process was used to synthesize and evaluate the ZIF gels for the high-throughput screening of the ZIF gel synthesis conditions (Fig. S1†). The screening criteria were as follows: (1) the gel should be wet before heat treatment, assuming that the bulk body is formed by the coating method, and (2) the gel should crystallize to the desired MOF by heat treatment. First, a solution containing the metal source, organic ligand, and base at a given concentration was prepared. The additional solvents were prepared separately. Each solution was dispensed into a 96-well plate (Thermo Fisher Scientific, material: polypropylene(PP)) in predetermined proportions using a Musashi Engineering automated pipetting device. The synthesis conditions are listed in Tables S1–S7.† After dispensing, the well plates were covered with sealing tape to prevent scattering and contamination. It was then mixed with Taitech micro mixer E-36 for 24 h. Subsequently, it was dried to remove the excess solvent for gelation. In the case of ethanol solvent, air drying was performed at room temperature, and in the case of DMF and deionized water, drying was performed in a 50 °C vacuum, both for 12 h. Morphological observations were made using an optical microscope equipped with an XY stage. See Fig. S2, S4, S6, S8, S10, S12, and S14† for the results. See the caption of Fig. S2† for the order in which the photos are arranged. In addition, gelation was determined by inverting the 96-well plate to check the fluidity. This method cannot determine the gel precisely because it cannot distinguish between viscous liquids;[60,61] however, it is often used because of its simplicity.[43,44,49] The samples were then heat-treated for crystallization at 120 °C for 48 h. X-ray diffraction (XRD) patterns were obtained for the candidate material at the bottom of each well using a high-throughput XRD measurement system equipped with a motorized stage. The synchrotron radiation facility in BL33XU (Toyota Beam Line) at SPring-8 (Hyogo, Japan) was used for the high-throughput XRD measurements.[62] The system settings are shown in Fig. S1.† A 96-well plate was attached to the sample holder on the XY stage. The XRD patterns were rapidly collected by scanning the XY stage with X-

ray irradiation at a wavelength of 0.8 Å (15.5 keV). The diffracted light was detected using a two-dimensional detector (PILATUS300K). The XRD patterns of each sample were calibrated using the PP peaks in the well plate. This method may not detect the pattern correctly if the film has strong orientations; however, our objective of screening the ZIF libraries was satisfactorily achieved. It was challenging to determine whether the desired MOF crystals had formed based on the XRD spectra. Therefore, we focused on the pattern, excluding well-plate-derived peaks, and each pattern was manually classified into groups of up to five based on their similarity. The XRD patterns obtained are shown in Fig. S3, S5, S7, S9, S11, S13, and S15.† Batch synthesis was performed under one of the synthetic conditions in each group, and more precise characterization was performed.

2.3 Batch synthesis of the ZIF gels

The optimal conditions for the gel synthesis of ZIF-zni and ZIF-61 were determined by screening and subsequent batch synthesis and evaluation. To the best of our knowledge, none of these have been previously reported. The ZIF-zni gel was synthesized using ethanol as a solvent, mixing zinc acetate (0.03 M, 30 ml) and imidazole (0.1 M, 40 ml), and stirring the mixture overnight at room temperature. Subsequently, the mixture was allowed to stand for 1 h. Then, 20 ml of the supernatant was extracted and dried at room temperature to obtain a transparent gel. To synthesize the ZIF-61 gel, ethanol was used as a solvent, and imidazole (0.1 M, 23 ml) and 2-methylimidazole (0.1 M, 3 ml) were mixed. Subsequently, zinc acetate (0.03 M, 30 ml) was mixed, and the mixture was stirred overnight in the atmosphere at room temperature. The mixture was then allowed to stand for 1 h. Following, the supernatant was removed, and the wet precipitate was dried overnight at room temperature.

2.4 Characterization of the ZIF gel

The shape of the particles contained in the gel was observed by scanning electron microscopy combined with energy-dispersive X-ray spectroscopy (SEM/EDX) using a Hitachi S-5500 instrument at an acceleration voltage of 2 kV. For this observation, we used a solvent-diluted gel that was dropped onto a Cu microgrid (Lacey microgrid, U1001) and dried overnight. Thermogravimetry/differential thermal analysis (TG/DTA) was performed in air over the temperature range from room temperature to 600 °C at a heating rate of 5 °C min^{-1} using a Rigaku D-DSC8230/TG8120IRH instrument with the gel placed on an aluminum pan. XRD analysis was performed with Rigaku Ultima IV using CuKα radiation with a step size of 0.02° and a scan speed of 10° min^{-1} to confirm that the resulting gel was a precursor that was coated on a glass substrate, heated to 150 °C, and solidified to yield the targeted MOF. A sample similarly coated and dried overnight at room temperature was also used for comparison.

2.5 Fabrication of the gel-derived ZIF films

Several substrates made of glass, fluorine-doped tin oxide (FTO), copper, and aluminum were used to fabricate the film. Approximately 0.1 ml of gel was dropped onto the substrate and spread by using a spin coater (Mikasa, Opticoat) operated at a rotational speed of 2000 rpm for a coating time of 20 s. The sample was then heated on a hot plate to 150 °C to solidify the gel.

2.6 Characterization of ZIF films

A nanoindentation test was performed using an Anton Paar Hit300 instrument to determine the mechanical properties of the film. For simple indentation, the maximum loads for ZIF-zni and ZIF-61 gels were 15 and 10 mN, respectively, and both the loading and unloading rates were 90 mN min^{-1}. Sinus loading was performed to obtain depth dependence of the mechanical properties. In sinus loading, the minimum load was 0.1 mN, the maximum loads were the same as those for simple indentation, the sinus frequency was 40 Hz, and the sinus amplitude was 3 mN. A diamond Berkovich indenter was used in both indentations. The obtained data were analyzed using the Oliver and Pharr method,[63] and the indentation Young's modulus (EIT) and indentation hardness (HIT) were calculated. In addition, the Poisson's ratio of the film was set at 0.2 in accordance with previously published research on ZIF.[41,64] SEM and EDX were used to observe the cross section of the film using a JEOL JSM-7000F and Hitachi High-Technology Regulus 8230, respectively. The accelerating voltages were 10 kV for SEM and 15 kV for EDX. For observation of glass and FTO substrates, the substrates for sample preparation were divided along with the film and the cross section was exposed. For observation of copper and aluminum substrates, after embedding them in epoxy resin, smooth cross sections were exposed using abrasive paper, alumina (average particle size: 0.3 μm), and colloidal silica (average particle size: 0.08 μm). CO_2 adsorption measurements were performed at a temperature of 0 °C and pressures up to 100 kPa using a Microtrac BELSORP-MAX analyzer. The ZIF-zni film was detached from the glass substrate to produce flake-like ZIF-zni, which was used in the subsequent measurements, while ZIF-zni crystal powder was utilized as a reference. It consisted of the sediment produced during the ZIF-zni gel synthesis, which was washed twice with ethanol, separated, and dried in a vacuum at 60 °C overnight. The sample holder was filled with the sample pre-evacuated at 150 °C in a vacuum overnight and mounted in the isothermal box of the instrument, which was maintained at 0 °C. The sample was evacuated prior to measurements.

2.7 Adhesion

Bonding was performed according to a previously described method.[56] Copper plates (Ra = 0.8) with dimensions of $\varphi 10 \times t5$ mm and $\varphi 5 \times t2$ mm were used to fabricate adhesive bodies for strength evaluation, and pieces of copper foil with $t10$ μm were also used to observe the cross-sectional structure. The adherends were ultrasonically cleaned with acetone for 10 min,

pickled with 7% diluted hydrochloric acid for 30 s, and dehydrated using acetone for 3 min. Using a small hot-pressing device equipped with a heater on the die, approximately 5 mg of the ZIF gel was applied to the adherend placed on the lower die, and the other adherend was placed on top and pressurized. The heating temperature of the die was 300 °C, the pressing force was 45 MPa, and the duration was 300 s.

2.8 Characterization of the adhesive body

A shear test was performed to evaluate the adhesive strength.[56] The φ10 copper plate side of the adhesive body was held, and a shear force was applied to the φ5 copper plate side of the adhesive body to destroy the adhesive body. The test was performed three times. The stroke speed was set to 1 mm min^{-1}, and the test was performed using a device that combined an Imada force gauge and an electric stage. SEM and EDX were used to observe the cross-sectional structures of the adhered foil with a JEOL JSM-7000F and Hitachi High-Technology Regulus 8230, respectively. The acceleration voltages were 10 kV and 15 kV for SEM and EDX, respectively. For observation, a film sample was cut at room temperature using an ultramicrotome (Leica Microsystems EM UC7i-FC) to expose the cross section.

2.9 Statistical modelling of the tendency of the wet gel

To evaluate the influence of each factor of the synthesis conditions on gelation, statistical modeling was performed on the wet gelation results from the high-throughput experiments. The binary random variable *Gel* indicates whether wet gelation occurred (1: gelation; 0: no gelation). To evaluate the pairwise relationships between the occurrence of gelation and the values of each factor, the average value of the *Gel* at each value of each factor was used for easy comprehension of the relationship. Each variable considered as a factor other than those defined in Tables S1–S7† is listed in Table 1. In addition, to evaluate the overall influence on the gelation tendency considering the correlation between each factor, logistic regression analysis was performed using the *Gel* as the objective variable and each factor as an explanatory variable. Categorical variables are coded as one-hot vectors. In the encoding, the states where M1 is ZnAc, M1_sol is ethanol, S1 is noadd (the state meaning no adding), B1 is noadd, and the system im–bim is set to zero. The variables were selected such that there was no linear dependence on the explanatory variables. Logistic regression analysis was performed using the glm function in the R package stats.

Table 1 Variables considered as factors for gelation tendency

Variable	Description
M1_sol	Solvent of M1
M1_vol	Volume of M1
L1_vol + L2_vol	Sum of the volume of L1 and L2
S1_vol	Volume of S1
B1_vol	Volume of B1
M1_CoAc	Whether M1 is CoAc or not (0 means M1 is ZnAc)
M1_sol_water	Whether solvent of M1 is water or not
M1_sol_DMF	Whether solvent of M1 is DMF or not
S1_EtOH	Whether solvent of S1 is EtOH or not
S1_water	Whether solvent of S1 is water or not
S1_DMF	Whether solvent of S1 is DMF or not
B1_NaOH	Whether solvent of B1 is NaOH or not
B1_KOH	Whether solvent of B1 is KOH or not
system_im–mim	Whether the synthesis system is im–mim or not
system_dcim	Whether the synthesis system is dcim or not
system_pr	Whether the synthesis system is pr or not
system_bim	Whether the synthesis system is bim or not
system_im	Whether the synthesis system is im or not

3 Results and discussion

This study investigated 473 experimental conditions, and the process from synthesis to evaluation took approximately two weeks. We characterized the newly discovered ZIF-zni gel using high-throughput screening (Fig. 1). The ZIF-zni gel was obtained by drying the supernatant from a clear colloidal solution (Fig. 1A and B). The solutes in this gel were nanoparticles with an average diameter of 132 nm (Fig. 1C and D). When this gel was heated, the excess ethanol evaporated and remained stable up to approximately 500 °C (Fig. 1E). It has been reported that ZIF-zni decomposes at about 500 °C, which is consistent with the present result.[65] Although a small peak was observed in the XRD pattern of the sample dried at room temperature, its intensity was relatively weak (Fig. 1F). However, significant crystallization occurred when this gel was solidified on a substrate heated to 150 °C. This suggests that the nanoparticles, which are solutes in the gel, are primarily amorphous precursors of ZIF-zni.

Forming MOF films directly on desired substrates is an essential but challenging task. Fig. 2 shows a cross-sectional SEM image of the film formed by coating and drying the ZIF-zni gel on a substrate. Dense films were formed on glass, FTO, Cu, and Al substrates. It is industrially important that ZIF-zni films can be formed on various substrates using this simple process. In addition, Fig. 3 shows the results of nanoindentation performed on the ZIF-zni film on the FTO. The ZIF-zni film recovered significantly upon unloading and remained elastically stable up to this loading level (Fig. 3A). A slight creep was observed after the maximum load was reached. This has also been confirmed by the nanoindentation of ZIF-zni single crystals.[64] In addition, from the profile of indentation Young's modulus and indentation hardness in the depth direction, the ZIF-zni film has an indentation Young's modulus of 18–22 GPa, an indentation hardness of 1.4–2.2 GPa, and excellent mechanical stability. This value is significantly higher than that of the ZIF-zni single crystal (7–9 GPa) in terms of indentation Young's modulus. The indentation moduli of single crystals and thin films or monoliths are often very different.[41,66,67] Surface roughness and elastic anisotropy have been proposed as the causes; however, clarifying the factors in the case of ZIF-zni films is a future challenge. The CO_2 adsorption properties of the film were also evaluated (Fig. S16†). Similar to the crystal powder, the ZIF-zni film has retained its gas adsorption capacity. However, the amount of CO_2 adsorbed per sorbent weight is three to four times smaller than that of the crystal powder, which is likely due to the presence of unreacted

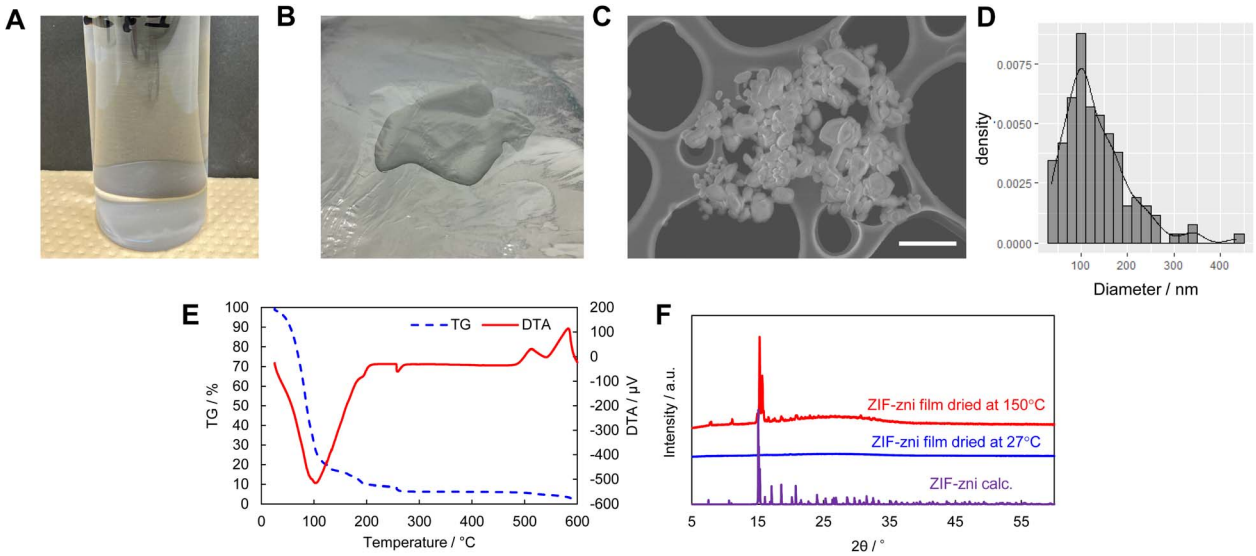

Fig. 1 Characterization of the ZIF-zni gel. (A) ZIF-zni colloidal solution. (B) ZIF-zni gel. (C) SEM images of ZIF-zni particles (scale bar: 1 μm). (D) Particle size distribution of the ZIF-zni gel. (E) Thermogravimetric analysis of the ZIF-zni gel. (F) XRD patterns of the ZIF-zni films.

imidazole or insufficient activation before adsorption related to the flaky shape of the film. ZIF-zni is chemically stable (Fig. S17†) and can be potentially used as a separator for propene/propane mixtures.[68] Thus, the coating technique utilizing the ZIF-zni gel may be employed in such applications.

A unique application of the recently reported ZIF gel is its use as a strong structural adhesive.[56] This is related to the adhesion strength of the gel-derived film to the substrate, which is an essential mechanical property for mounting MOF devices. Therefore, a similar method was used in this study to bond a Cu substrate (Fig. 4A). Observation of the cross section of the adhesive body showed that the ZIF-zni gel was in close contact with the upper and lower copper substrates (Fig. 4B). This adhesive body had considerable strength (Fig. 4C), with an

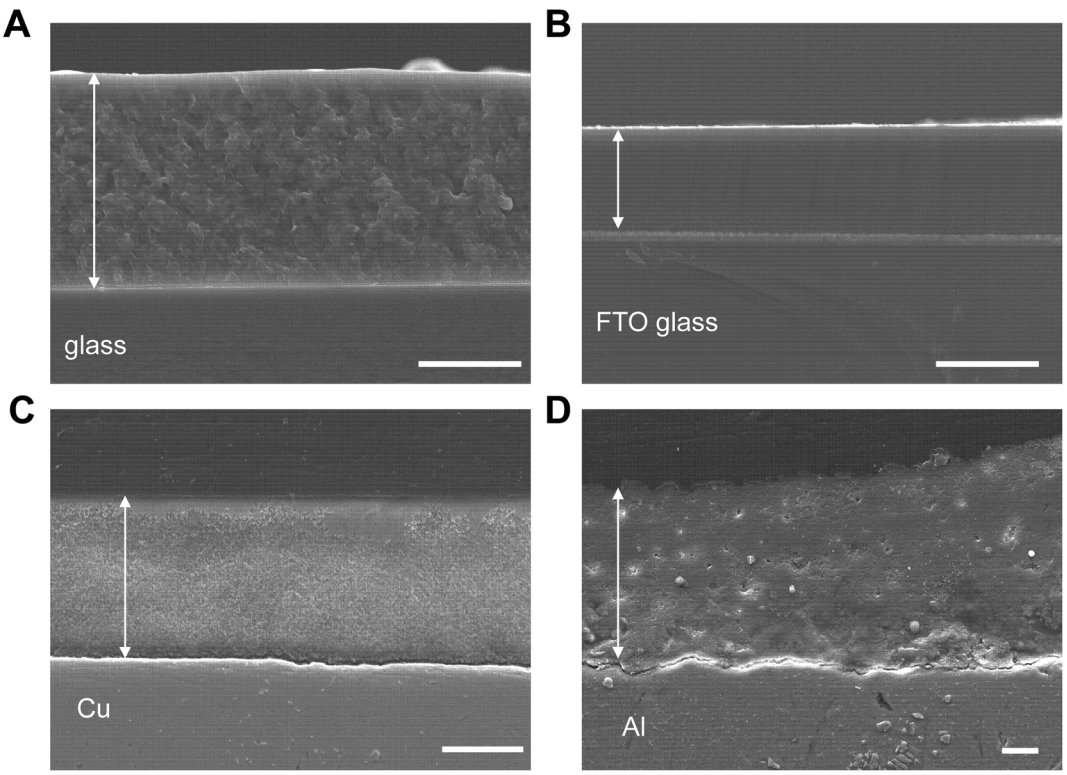

Fig. 2 Cross-sectional SEM images of ZIF-zni films on different substrates. (A) Glass. (B) FTO glass. (C) Cu. (D) Al. Scale bars: 5 μm.

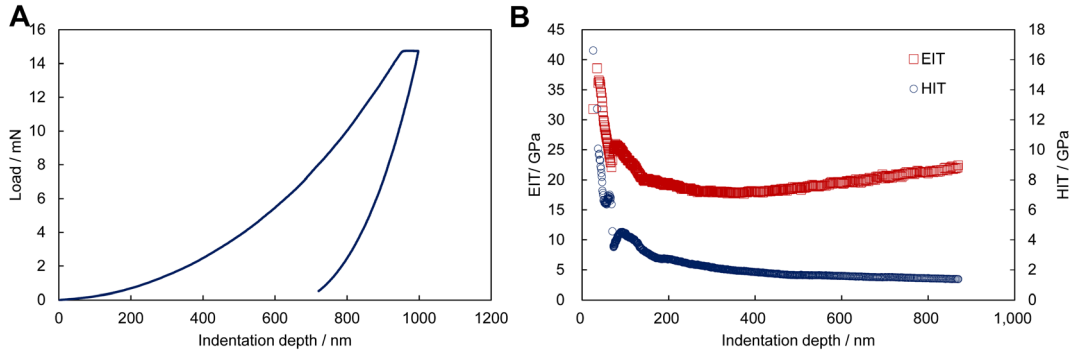

Fig. 3 Nanoindentation data of ZIF-zni films. (A) Representative load–displacement curve. (B) Indentation elastic moduli (EIT) and hardness (HIT) as a function of indentation depth.

average strength of 39.1 MPa (±3.9). This value was much higher than that of the ZIF-67 gel reported in a previous study at the same pressure (approximately 30 MPa).[56] The factors governing the shear strength in MOF bonding are not fully understood; however, it is thought that the hardness of the adhesive layer has an effect.[56] ZIF-zni has the highest single-crystal hardness among ZIFs of approximately 1 GPa,[64] and the hardness of the ZIF-zni film (1.4–2.2 GPa) is significantly higher than the hardness of the ZIF-67 gel-cured layer without pressure (0.1 GPa) obtained in a previous study.[56] Thus, the hardness of the ZIF-zni adhesive layer is expected to exceed that of the ZIF-67 adhesive layer reported previously, which may

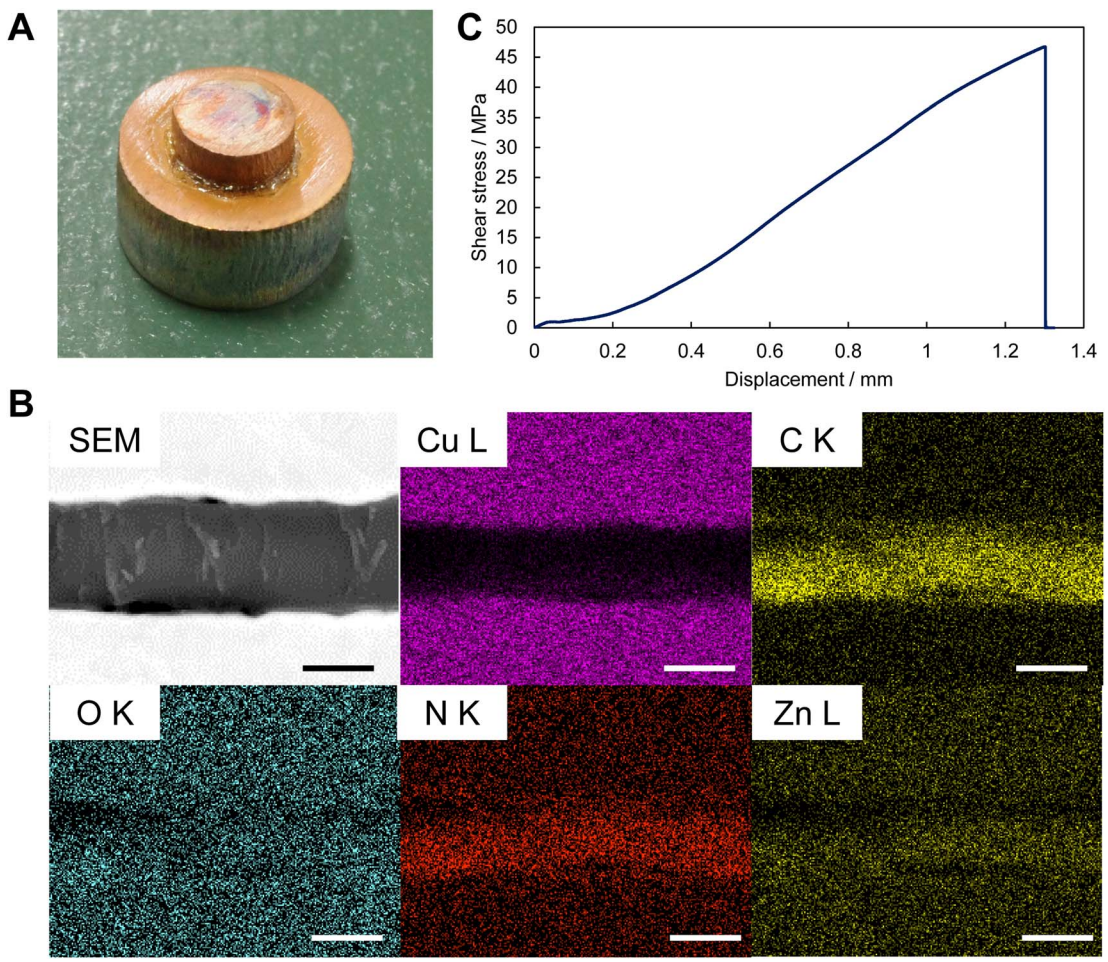

Fig. 4 Adhesive characterization of the ZIF-zni gel. (A) Photograph of the adhesive body. (B) Cross-sectional SEM image and EDX analysis of the adhesive body. Scale bar: 1 μm. (C) Stress-displacement curve of the adhesive body.

endow the ZIF-zni adhesive with a high shear strength. Therefore, an MOF with even a higher hardness may be used to further improve the adhesive properties.

In general, the conditions for forming MOF gels are not fully understood, and no unified strategy for forming MOF gels has been proposed. To obtain the desired MOF gel, it is necessary to form a wet gel before heat treatment and the desired MOF crystal by heat treatment. Although only wet gel was used to judge the gel at the screening stage in the high-throughput experiment conducted in this study, it is helpful to analyze these data and consider the influence of each factor on wet gelation to formulate a unified strategy for the formation of MOF gels. Fig. 5 shows the average value of the random variable *Gel* in each synthetic system. It can be seen that the gelation tendency differs greatly depending on the synthesis system. In particular, im and im–mim systems are prone to gelation. The nim–dmbim system also appeared to gel more likely; however, this system used DMF as the solvent, which may be due to solvent effects. Regarding the effects of metal ions, Zn appeared to gel more likely (Fig. 6A). However, in the nim–dmbim system, the effect of the individual metal ions on the gelation tendency was almost the same. Regarding the effect of the amount of the metal source, it appeared that the smaller the amount, the more likely it was to gel (Fig. 6B). This was particularly noticeable for nim–dmbim. Regarding the effect of the solvent, gelation seems to be easier when DMF is added (Fig. 6C). However, as mentioned above, this effect cannot be separated from the individual effects of the nim–dmbim system using the present data. The effects of ethanol and water appear to be very different, depending on the system. In the bim system, water appeared to gel more likely, whereas ethanol appeared to gel more likely in the im–mim system. Regarding the effect of the amount of organic ligands, there was a tendency for gelation to occur more likely as the amount of organic ligands increased (Fig. 6D). This is particularly evident for nim–dmbim. Regarding the influence of base, gelation was more likely to occur when KOH was added (Fig. 6E). However, in the im–mim system, almost no difference was observed between KOH, NaOH, and noadd. Regarding the effect of the base amount, the larger the base amount, the more likely it was to gel. However, this effect was insignificant (Fig. 6F).

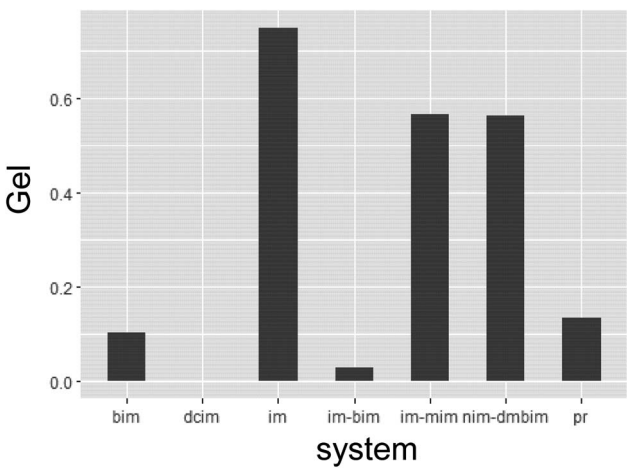

Fig. 5 Dependence on the synthesis system of the wet-gel tendency.

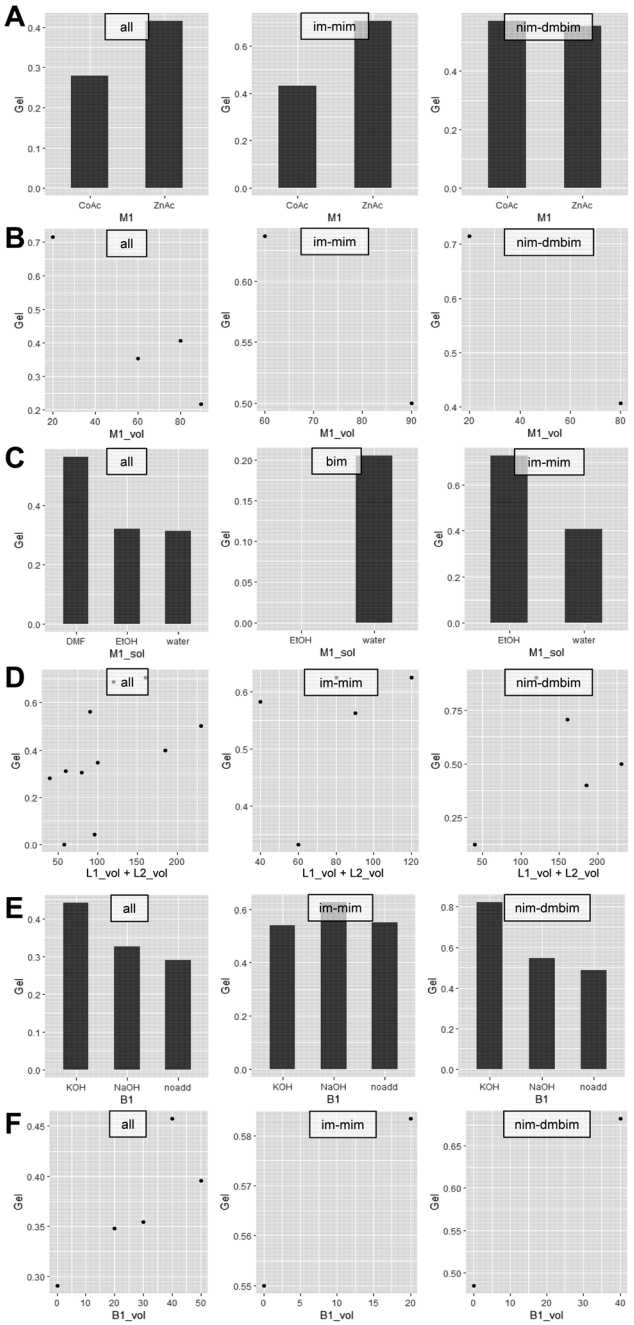

Fig. 6 Wet-gel tendency's dependence on different factors (A) M1. (B) M1_vol. (C) M1_sol. (D) L1_vol + L2_vol. (E) B1. (F) B1_vol.

Regarding the relationship between the gelation tendency and the factors described above, statistical significance was confirmed by further statistical modeling considering the correlation between the factors. Table 2 presents the fitting results obtained using the logistic regression model. The accuracy of this model was 0.84, indicating that it learned well. Regarding the estimated values of each partial regression

Table 2 Results of the logistic regression modelling of wet-gel fabrication[a]

	Estimate	Std. error	z Value	Pr(>|z|)	Signif. codes
(Intercept)	−0.586454	1.161134	−0.505	0.61351	·
M1_vol	**−0.049936**	**0.011612**	**−4.3**	**1.70×10^{-5}**	***
L1_vol + L2_vol	**0.021568**	**0.005671**	**3.803**	**0.00014**	***
S1_vol	−0.001754	0.033696	−0.052	0.958491	
B1_vol	0.01613	0.021138	0.763	0.445423	
M1_CoAc	**−1.224894**	**0.290284**	**−4.22**	**2.45×10^{-5}**	***
M1_sol_water	**−1.204256**	**0.413488**	**−2.912**	**0.00359**	**
M1_sol_DMF	−0.183335	1.095168	−0.167	0.867053	
S1_EtOH	0.67487	1.881998	0.359	0.7199	
S1_water	0.683437	1.75549	0.389	0.697044	
S1_DMF	1.334753	1.710685	0.78	0.435247	
B1_NaOH	0.241136	0.788782	0.306	0.759828	
B1_KOH	1.312142	0.793436	1.654	0.098179	.
system_im–mim	**3.263116**	**0.801371**	**4.072**	**4.66×10^{-5}**	***
system_dcim	−17.654868	896.719174	−0.02	0.984292	
system_pr	−0.901757	1.010027	−0.893	0.371962	
system_bim	−0.790544	0.965826	−0.819	0.413062	
system_im	**3.411591**	**0.889581**	**3.835**	**0.00013**	***

[a] Signif. codes: 0 '***' 0.001 '**' 0.01 '*' 0.05 '.' 0.1 ' ' 1.

coefficient, M1_vol and L1_vol + L2_vol are statistically significant as negative and positive estimates, respectively; the lower the amount of metal source and the higher the amount of organic ligand, the more the gel. Furthermore, owing to the influence of the metal ions, M1_CoAc had a negative estimated value, suggesting that Co is less likely to gel than Zn. Furthermore, as an influence of the solvent, M1_sol_water was estimated to have a negative value, suggesting that water has a lower tendency to gel than ethanol. In contrast, Fig. 6C shows that the gelation tendency was higher when the solvent was DMF, but no statistically significant difference was detected. In addition, system_im–mim and system_im had positive estimated values, suggesting that the gelation tendency was higher in the im or im–mim systems than in the im–bim system. In this high-throughput screening, in the im–bim system, for example, we were unable to find the gel synthesis conditions that would allow the formation of the desired MOF crystals; however, wet gels could not be formed under many conditions. From the statistical modeling results above, it is possible to form a wet gel by changing the range of experimental conditions, for example, by decreasing the amount of the metal source and increasing the amount of the organic ligand.

The ZIF-61 gel is another ZIF gel discovered in this study through high-throughput screening. In addition to the ZIF-zni gel, a similar characterization was performed on the ZIF-61 gel-derived film and adhesive (Fig. S18–S21†). The results showed that it was possible to form dense and mechanically rigid films on multiple substrates using the ZIF-61 gel and that the adhesive strength was equivalent to that of the ZIF-67 gel in previous research.[56] ZIF-61 can be potentially utilized as a catalyst for manufacturing tetrahydrofuran.[69] Thus, the coating technique using the novel ZIF-61 gel may be employed for such an application.

4 Conclusions

For the ZIF gel synthesis using acetate, we efficiently searched for gelation conditions targeting multiple ZIFs using high-throughput screening, followed by batch synthesis. Consequently, we discovered the ZIF-zni and ZIF-61 gels as novel ZIF gels. This gel can form a dense and rigid film on multiple substrates upon coating and drying. This process has excellent industrial feasibility, and the results are important for applying ZIF-zni and ZIF-61 films on the desired substrates.

As a unique application, we investigated the potential of the obtained ZIF-zni and ZIF-61 gels as structural adhesives for metals. Consequently, the shear strength of the adhesive exceeded 30 MPa. This value exceeds those of previously reported MOF adhesives. Furthermore, using data obtained from high-throughput screening experiments, we evaluated the influence of the synthesis conditions on the wet gel formation conditions, which are important for the realization of gel-based films and adhesives, through statistical modeling using logistic regression. The following statistically significant trends were found: the wet gelation tendency was high when (i) using a smaller amount of metal source or a larger amount of organic ligand, (ii) using Zn^{2+} more than Co^{2+} as the metal ion, and (iii) using ethanol more than water as the solvent. This is a crucial suggestion for finding widely applicable conditions for wet gelation, and more detailed research on its applicability and mechanism, including ZIFs and MOFs other than ZIFs, which were not targeted in this study, should be conducted in future studies.

Author contributions

I. M. and M. U. conceived the project. All the authors conducted the experiments. I. M. and M. U. prepared the manuscript. All the authors discussed the results and approved the final version of the manuscript.

Conflicts of interest

The authors declare no competing financial interest.

Acknowledgements

High-throughput XRD measurements were performed using the BL33XU beamline at SPring-8 (Hyogo, Japan) with the approval of the Japan Synchrotron Radiation Research Institute (Proposal No. 2022A7030 and 2022B7030). We appreciate the help of Dr Shin Tajima in conducting the XRD measurements. We also thank Dr Akitoshi Suzumura for the fruitful discussions and advice. We also thank Mr Takuto Iwai for the experimental help and advice.

References

1 J. B. Goodenough, Electrochemical energy storage in a sustainable modern society, *Energy Environ. Sci.*, 2014, **7**, 14–18.
2 M. M. Thackeray, C. Wolverton and E. D. Isaacs, Electrical energy storage for transportation—approaching the limits of, and going beyond, lithium-ion batteries, *Energy Environ. Sci.*, 2012, **5**, 7854–7863.
3 Z. Liang, R. Zhao, T. Qiu, R. Zou and Q. Xu, Metal-organic framework-derived materials for electrochemical energy applications, *EnergyChem*, 2019, **1**, 100001.
4 Y. Zhao, Z. Song, X. Li, Q. Sun, N. Cheng, S. Lawes and X. Sun, Metal organic frameworks for energy storage and conversion, *Energy Storage Mater.*, 2016, **2**, 35–62.
5 X. Zhang, A. Chen, M. Zhong, Z. Zhang, X. Zhang, Z. Zhou and X.-H. Bu, Metal–organic frameworks (MOFs) and MOF-derived materials for energy storage and conversion, *Electrochem. Energy Rev.*, 2018, **2**, 29–104.
6 I. Hussain, S. Iqbal, C. Lamiel, A. Alfantazi and K. Zhang, Recent advances in oriented metal–organic frameworks for supercapacitive energy storage, *J. Mater. Chem. A*, 2022, **10**, 4475–4488.
7 V. Bon, Metal-organic frameworks for energy-related applications, *Curr. Opin. Green Sustainable Chem.*, 2017, **4**, 44–49.
8 H. Wang, Q.-L. Zhu, R. Zou and Q. Xu, Metal-organic frameworks for energy applications, *Chem*, 2017, **2**, 52–80.
9 G. Xu, P. Nie, H. Dou, B. Ding, L. Li and X. Zhang, Exploring metal organic frameworks for energy storage in batteries and supercapacitors, *Mater. Today*, 2017, **20**, 191–209.
10 A. E. Baumann, D. A. Burns, B. Liu and V. S. Thoi, Metal-organic framework functionalization and design strategies for advanced electrochemical energy storage devices, *Commun. Chem.*, 2019, **2**, 86.
11 C. C. Hou and Q. Xu, Metal–organic frameworks for energy, *Adv. Energy Mater.*, 2018, **9**, 1801307.
12 T. Qiu, Z. Liang, W. Guo, H. Tabassum, S. Gao and R. Zou, Metal–organic framework-based materials for energy conversion and storage, *ACS Energy Lett.*, 2020, **5**, 520–532.
13 P. Küsgens, A. Zgaverdea, H.-G. Fritz, S. Siegle and S. Kaskel, Metal-organic frameworks in monolithic structures, *J. Am. Ceram. Soc.*, 2010, **93**, 2476–2479.
14 J. Ren and B. C. North, Shaping porous materials for hydrogen storage applications: A review, *J. Technol. Innovations Renewable Energy*, 2014, **3**, 12–20.
15 R. N. Widmer, G. I. Lampronti, B. Kunz, C. Battaglia, J. H. Shepherd, S. A. T. Redfern and T. D. Bennett, Manufacturing macroporous monoliths of microporous metal–organic frameworks, *ACS Appl. Nano Mater.*, 2018, **1**, 497–500.
16 I. Miyazaki, Y. Masuoka, A. Suzumura, S. Moribe and M. Umehara, Direct sintering behavior of metal organic frameworks/coordination polymers, *ACS Omega*, 2022, **7**, 47906–47911.
17 O. Shekhah, H. Wang, S. Kowarik, F. Schreiber, M. Paulus, M. Tolan, C. Sternemann, F. Evers, D. Zacher, R. A. Fischer and C. Wöll, Step-by-step route for the synthesis of metal-organic frameworks, *J. Am. Chem. Soc.*, 2007, **129**, 15118–15119.
18 K. Otsubo, T. Haraguchi, O. Sakata, A. Fujiwara and H. Kitagawa, Step-by-step fabrication of a highly oriented crystalline three-dimensional pillared-layer-type metal–organic framework thin film confirmed by synchrotron X-ray diffraction, *J. Am. Chem. Soc.*, 2012, **134**, 9605–9608.
19 J. Yao and H. Wang, Zeolitic imidazolate framework composite membranes and thin films: Synthesis and applications, *Chem. Soc. Rev.*, 2014, **43**, 4470–4493.
20 P. Falcaro, K. Okada, T. Hara, K. Ikigaki, Y. Tokudome, A. W. Thornton, A. J. Hill, T. Williams, C. Doonan and M. Takahashi, Centimetre-scale micropore alignment in oriented polycrystalline metal-organic framework films via heteroepitaxial growth, *Nat. Mater.*, 2017, **16**, 342–348.
21 Y. Liu, E. Hu, E. A. Khan and Z. Lai, Synthesis and characterization of ZIF-69 membranes and separation for CO_2/CO mixture, *J. Membr. Sci.*, 2010, **353**, 36–40.
22 H. Ji, S. Hwang, K. Kim, C. Kim and N. C. Jeong, Direct in situ conversion of metals into metal–organic frameworks: A strategy for the rapid growth of MOF films on metal substrates, *ACS Appl. Mater. Interfaces*, 2016, **8**, 32414–32420.
23 H. Guo, G. Zhu, I. J. Hewitt and S. Qiu, "Twin copper source" growth of metal−organic framework membrane: $Cu_3(BTC)_2$ with high permeability and selectivity for recycling H_2, *J. Am. Chem. Soc.*, 2009, **131**, 1646–1647.
24 K. Khaletskaya, S. Turner, M. Tu, S. Wannapaiboon, A. Schneemann, R. Meyer, A. Ludwig, G. Van Tendeloo and R. A. Fischer, Self-directed localization of ZIF-8 thin film formation by conversion of ZnO nanolayers, *Adv. Funct. Mater.*, 2014, **24**, 4804–4811.
25 A. Demessence, C. Boissière, D. Grosso, P. Horcajada, C. Serre, G. Férey, G. J. A. A. Soler-Illia and C. Sanchez, Adsorption properties in high optical quality nanoZIF-8 thin films with tunable thickness, *J. Mater. Chem.*, 2010, **20**, 7676–7681.
26 Z. Chen, R. Wang, T. Ma, J. L. Wang, Y. Duan, Z. Z. Dai, J. Xu, H. J. Wang, J. Yuan, H. L. Jiang, Y. W. Yin, X. G. Li, M. R. Gao and S. H. Yu, Large-area crystalline zeolitic imidazolate

framework thin films, *Angew. Chem., Int. Ed.*, 2021, **60**, 14124–14130.
27 I. Stassen, M. Styles, G. Grenci, H. V. Gorp, W. Vanderlinden, S. D. Feyter, P. Falcaro, D. D. Vos, P. Vereecken and R. Ameloot, Chemical vapour deposition of zeolitic imidazolate framework thin films, *Nat. Mater.*, 2016, **15**, 304–310.
28 S. Qiu, M. Xue and G. Zhu, Metal–organic framework membranes: From synthesis to separation application, *Chem. Soc. Rev.*, 2014, **43**, 6116–6140.
29 W. Li, Metal–organic framework membranes: Production, modification, and applications, *Prog. Mater. Sci.*, 2019, **100**, 21–63.
30 Y. S. Lin, Metal organic framework membranes for separation applications, *Curr. Opin. Chem. Eng.*, 2015, **8**, 21–28.
31 Z. Kang, L. Fan and D. Sun, Recent advances and challenges of metal–organic framework membranes for gas separation, *J. Mater. Chem. A*, 2017, **5**, 10073–10091.
32 L. Y. Molefe, N. M. Musyoka, J. Ren, H. W. Langmi, M. Mathe and P. G. Ndungu, Polymer-based shaping strategy for zeolite templated carbons (ZTC) and their metal organic framework (MOF) composites for improved hydrogen storage properties, *Front. Chem.*, 2019, **7**, 864.
33 L. Y. Molefe, N. M. Musyoka, J. Ren, H. W. Langmi, P. G. Ndungu, R. Dawson and M. Mathe, Synthesis of porous polymer-based metal–organic frameworks monolithic hybrid composite for hydrogen storage application, *J. Mater. Sci.*, 2019, **54**, 7078–7086.
34 R. Ostermann, J. Cravillon, C. Weidmann, M. Wiebcke and B. M. Smarsly, Metal–organic framework nanofibers via electrospinning, *Chem. Commun.*, 2011, **47**, 442–444.
35 S. Basu, M. Maes, A. Cano-Odena, L. Alaerts, D. E. De Vos and I. F. J. Vankelecom, Solvent resistant nanofiltration (SRNF) membranes based on metal-organic frameworks, *J. Membr. Sci.*, 2009, **344**, 190–198.
36 K. Díaz, L. Garrido, M. López-González, L. F. del Castillo and E. Riande, CO_2 transport in polysulfone membranes containing zeolitic imidazolate frameworks as determined by permeation and PFG NMR techniques, *Macromolecules*, 2009, **43**, 316–325.
37 Q. Zhang, H. Yang, T. Zhou, X. Chen, W. Li and H. Pang, Metal-organic frameworks and their composites for environmental applications, *Adv. Sci.*, 2022, **9**, 2204141.
38 Y. Xue, S. Zheng, H. Xue and H. Pang, Metal–organic framework composites and their electrochemical applications, *J. Mater. Chem. A*, 2019, **7**, 7301–7327.
39 Q. L. Zhu and Q. Xu, Metal-organic framework composites, *Chem. Soc. Rev.*, 2014, **43**, 5468–5512.
40 D. Bazer-Bachi, L. Assié, V. Lecocq, B. Harbuzaru and V. Falk, Towards industrial use of metal-organic framework: Impact of shaping on the MOF properties, *Powder Technol.*, 2014, **255**, 52–59.
41 T. Tian, J. Velazquez-Garcia, T. D. Bennett and D. Fairen-Jimenez, Mechanically and chemically robust ZIF-8 monoliths with high volumetric adsorption capacity, *J. Mater. Chem. A*, 2015, **3**, 2999–3005.
42 J.-W. Ye, X. Zhou, Y. Wang, R.-K. Huang, H.-L. Zhou, X.-N. Cheng, Y. Ma and J.-P. Zhang, Room-temperature sintered metal-organic framework nanocrystals: A new type of optical ceramics, *Sci. China Mater.*, 2018, **61**, 424–428.
43 H. Wang, B. H. Chen and D. J. Liu, Metal-organic frameworks and metal-organic gels for oxygen electrocatalysis: Structural and compositional considerations, *Adv. Mater.*, 2021, **33**, 2008023.
44 S. Saha, J. Bachl, T. Kundu, D. D. Diaz and R. Banerjee, Amino acid-based multiresponsive low-molecular weight metallohydrogels with load-bearing and rapid self-healing abilities, *Chem. Commun.*, 2014, **50**, 3004–3006.
45 S. Saha, E.-M. Schön, C. Cativiela, D. Díaz Díaz and R. Banerjee, Proton-conducting supramolecular metallogels from the lowest molecular weight assembler ligand: A quote for simplicity, *Chem.–Eur. J.*, 2013, **19**, 9562–9568.
46 A. Mallick, E.-M. Schön, T. Panda, K. Sreenivas, D. D. Díaz and R. Banerjee, Fine-tuning the balance between crystallization and gelation and enhancement of CO_2 uptake on functionalized calcium based MOFs and metallogels, *J. Mater. Chem.*, 2012, **22**, 14951–14963.
47 H. B. Aiyappa, S. Saha, P. Wadge, R. Banerjee and S. Kurungot, Fe(III) phytate metallogel as a prototype anhydrous, intermediate temperature proton conductor, *Chem. Sci.*, 2015, **6**, 603–607.
48 B. Bueken, N. Van Velthoven, T. Willhammar, T. Stassin, I. Stassen, D. A. Keen, G. V. Baron, J. F. M. Denayer, R. Ameloot, S. Bals, D. De Vos and T. D. Bennett, Gel-based morphological design of zirconium metal-organic frameworks, *Chem. Sci.*, 2017, **8**, 3939–3948.
49 T. Tian, Z. Zeng, D. Vulpe, M. E. Casco, G. Divitini, P. A. Midgley, J. Silvestre-Albero, J. C. Tan, P. Z. Moghadam and D. Fairen-Jimenez, A sol-gel monolithic metal-organic framework with enhanced methane uptake, *Nat. Mater.*, 2018, **17**, 174–179.
50 M. Tricarico and J.-C. Tan, Mechanical properties and nanostructure of monolithic zeolitic imidazolate frameworks: A nanoindentation, nanospectroscopy, and finite element study, *Mater. Today Nano*, 2022, **17**, 100166.
51 P. Liao, H. Fang, J. Zhang, Y. Hu, L. Chen and C. Y. Su, Transforming HKUST-1 metal–organic frameworks into gels – Stimuli-responsiveness and morphology evolution, Eur, *J. Inorg. Chem.*, 2017, **2017**, 2580–2584.
52 G. J. H. Lim, Y. Wu, B. B. Shah, J. J. Koh, C. K. Liu, D. Zhao, A. K. Cheetham, J. Wang and J. Ding, 3D-printing of pure metal–organic framework monoliths, *ACS Mater. Lett.*, 2019, **1**, 147–153.
53 S. M. F. Vilela, P. Salcedo-Abraira, L. Micheron, E. L. Solla, P. G. Yot and P. Horcajada, A robust monolithic metal-organic framework with hierarchical porosity, *Chem. Commun.*, 2018, **54**, 13088–13091.
54 L. Li, S. Xiang, S. Cao, J. Zhang, G. Ouyang, L. Chen and C. Y. Su, A synthetic route to ultralight hierarchically micro/mesoporous Al(III)-carboxylate metal-organic aerogels, *Nat. Commun.*, 2013, **4**, 1774.

55 M. R. Lohe, M. Rose and S. Kaskel, Metal-organic framework (MOF) aerogels with high micro- and macroporosity, *Chem. Commun.*, 2009, **40**, 6056–6058.

56 E. Hunter-Sellars, P. A. Saenz-Cavazos, A. R. Houghton, S. R. McIntyre, I. P. Parkin and D. R. Williams, Sol–gel synthesis of high-density zeolitic imidazolate framework monoliths via ligand assisted methods: Exceptional porosity, hydrophobicity, and applications in vapor adsorption, *Adv. Funct. Mater.*, 2020, **31**, 2008357.

57 J. Hou, A. F. Sapnik and T. D. Bennett, Metal-organic framework gels and monoliths, *Chem. Sci.*, 2020, **11**, 310–323.

58 C. Duan, Y. Yu, J. Li, L. Li, B. Huang, D. Chen and H. Xi, Recent advances in the synthesis of monolithic metal-organic frameworks, *Sci. China Mater.*, 2021, **64**, 1305–1319.

59 H. H. M. Yeung, A. F. Sapnik, F. Massingberd-Mundy, M. W. Gaultois, Y. Wu, D. A. X. Fraser, S. Henke, R. Pallach, N. Heidenreich, O. V. Magdysyuk, N. T. Vo and A. L. Goodwin, Control of metal-organic framework crystallization by metastable intermediate pre-equilibrium species, *Angew. Chem., Int. Ed.*, 2019, **58**, 566–571.

60 A. K. Chaudhari, I. Han and J. C. Tan, Multifunctional supramolecular hybrid materials constructed from hierarchical self-ordering of in situ generated metal-organic framework (MOF) nanoparticles, *Adv. Mater.*, 2015, **27**, 4438–4446.

61 I. Miyazaki, Y. Masuoka, A. Ohshima, N. Takahashi, A. Suzumura, S. Moribe, H. Takao and M. Umehara, Sintering metal-organic framework gels for application as structural adhesives, *Small*, 2023, **19**, 2300298.

62 S. K. Suram, P. F. Newhouse and J. M. Gregoire, High throughput light absorber discovery, Part 1: An algorithm for automated Tauc analysis, *ACS Comb. Sci.*, 2016, **18**, 673–681.

63 A. Benayad, D. Diddens, A. Heuer, A. N. Krishnamoorthy, M. Maiti, F. L. Cras, M. Legallais, F. Rahmanian, Y. Shin, H. Stein, M. Winter, C. Wölke, P. Yan and I. Cekic-Laskovic, High-throughput experimentation and computational freeway lanes for accelerated battery electrolyte and interface development research, *Adv. Energy Mater.*, 2022, **12**, 2102678.

64 Y. Yao, Z. Huang, T. Li, H. Wang, Y. Liu, H. S. Stein, Y. Mao, J. Gao, M. Jiao, Q. Dong, J. Dai, P. Xie, H. Xie, S. D. Lacey, I. Takeuchi, J. M. Gregoire, R. Jiang, C. Wang, A. D. Taylor, R. Shahbazian-Yassar and L. Hu, High-throughput, combinatorial synthesis of multimetallic nanoclusters, *Proc. Natl. Acad. Sci. U. S. A.*, 2020, **117**, 6316–6322.

65 S. Bauer, C. Serre, T. Devic, P. Horcajada, P. Marrot, J. Ferey and N. Stock, High-throughput assisted rationalization of the formation of metal organic frameworks in the iron (III) aminoterephthalate solvothermal system, *Inorg. Chem.*, 2008, **47**, 7568–7576.

66 M. L. Kelty, W. Morris, A. T. Gallagher, J. S. Anderson, K. A. Brown, C. A. Mirkin and T. D. Harris, High-throughput synthesis and characterization of nanocrystalline porphyrinic zirconium metal-organic frameworks, *Chem. Commun.*, 2016, **52**, 7854–7857.

67 R. Banerjee, A. Phan, B. Wang, C. Knobler, H. Furukawa, M. O'Keeffe and O. M. Yaghi, High-throughput synthesis of zeolitic imidazolate frameworks and application to CO_2 capture, *Science*, 2008, **319**, 939–943.

68 M. Hovestadt, S. Friebe, L. Helmich, M. Lange, J. Mollmer, R. Glaser, A. Mundstock and M. Hartmann, Continuous separation of light olefin/paraffin mixtures on ZIF-4 by pressure swing adsorption and membrane permeation, *Molecules*, 2018, **23**, 889.

69 Y. Wang, X. Lang and S. Fan, Accelerated nucleation of tetrahydrofuran (THF) hydrate in presence of ZIF-61, *J. Nat. Gas Chem.*, 2012, **21**, 299–301.